Am J Cancer Res 2026;16(6):2109-2130
www.ajcr.us /ISSN:2156-6976/ajcr0172084

*Original Article*

# Unc-51 like kinase 3 induces reticulophagy by mediating the GLI1/CAMK2B signaling pathway to promote the malignant progression of prostate cancer

Qin-Quan Wang[1,2], Chen Sun[2], Jin-Hua Wu[3], Dong-Dong Yu[1], Hui-Liang Zhou[1]

*[1]Department of Andrology and Sexual Medicine, The First Affiliated Hospital of Fujian Medical University, 20 Chazhong Road, Fuzhou 350005, Fujian, China; [2]The First Affiliated Hospital of Wenzhou Medical University, Wenzhou 325016, Zhejiang, China; [3]Department of Andrology, Ganzhou People's Hospital of Jiangxi Province, No. 17 Hongqi Avenue, Ganzhou 341000, Jiangxi, China*

Received February 12, 2026; Accepted May 9, 2026; Epub June 15, 2026; Published June 30, 2026

**Abstract:** Recent studies have found that the reticulophagy pathway is able to clear excess endoplasmic reticulum to protect cells from endoplasmic reticulum stress-induced damage. The role of reticulophagy in prostate cancer is still unknown. Key genes of reticulophagy were studied. Subsequently, the ULK3 and CAMK2B mRNA levels were confirmed. ULK3 and CAMK2B expression were elevated in prostate cancer tissues. The silencing of ULK3 inhibited prostate cancer cell vitality. The overexpression of ULK3 had the opposite effect. ULK3 was able to enhance the CAMK2B protein expression by promoting the entry of GLI1 into the nucleus, thereby upregulating the level of reticulophagy. Knockdown of CAMK2B could inhibit reticulophagy induced by ULK3. Further experiments showed that ULK3 phosphorylated GLI1, promoted its nuclear entry and binding to the CAMK2B promoter to enhance CAMK2B expression. Down-regulation of ULK3 inhibited the growth of prostate cancer vitality in vivo. This study confirmed that ULK3 promoted the prostate cancer by upregulating GLI1/CAMK2B-induced reticulophagy.

**Keywords:** ULK3, CAMK2B, GLI1, endoplasmic reticulum autophagy, prostate cancer

## Introduction

Prostate cancer is the second most common cancer among men worldwide, occurs most frequently in middle-aged men aged 45-60 years, and is one of the most common malignancies among the leading causes of cancer-related mortality [1-3]. Data showed that an estimated 1.6 million cases of prostate cancer are reported each year, and about 300,000 people die from the disease each year [4, 5]. At present, the main methods for diagnosing prostate cancer include physical examination, imaging tests, and chemotherapy is the preferred method for treating patients with prostate cancer, but there is a serious risk of drug resistance in current chemotherapy modalities [6]. It is undeniable that prostate cancer is still a major medical problem for men. Therefore, finding therapeutic targets for prostate cancer is a top priority for the treatment of prostate cancer.

The ER selects autophagy pathway to undergoes continuous remodeling, known as Reticulophagy (ER-phagy) [7]. ER-phagy promotes cellular homeostasis or apoptosis, and has been found to have a regulatory effect on tumorigenesis, which enhances the survival of cancer cells by improving the function of ER in response to hypoxia and other damaging stimuli [7]. ER-phagy also exerts important function in the invasion, metastasis, and drug resistance of tumor cells. Inhibiting ER-phagy can enhance the sensitivity of cancer cells to chemotherapy drugs, affecting their migration [8-11]. However, the role of ER-phagy in prostate cancer and its mechanism are not well understood.

ULK3 (Unc51-like kinase 3) is an uncharacterized member of the ULK1-4 kinase family which is thought to have effects similar to those of Drosophila fusion kinases in mammalian cells [12]. ULK1 is the most studied molecule in the

https://doi.org/10.62347/0TBP6619

**Table 1.** The clinicopathologic characteristics in twelve prostate cancer patients

| Characteristics | Group | Case number | CR (%) |
|---|---|---|---|
| Age | ≤ 60 | 5 | 41.7 |
| | > 60 | 7 | 58.3 |
| Gleason score | ≤ 6 | 2 | 16.6 |
| | 7 | 5 | 41.7 |
| | ≥ 8 | 5 | 41.7 |
| cN stage | N0 | 10 | 83.3 |
| | N1 | 2 | 16.7 |
| cM stage | M0 | 12 | 100 |
| | M1 | 0 | 0 |
| pT stage | 2 | 9 | 75 |
| | 3-4 | 3 | 25 |
| Preoperative PSA | < 10 | 7 | 58.3 |
| | 10-20 | 3 | 25 |
| | > 20 | 2 | 16.7 |

CR: Composition ratio.

family. However, there is little information about the role and mechanism of ULK3. Hedgehog signaling plays an important role in the growth of embryonic development and cell proliferation. ULK3 is considered to be a positive regulator of Hedgehog signaling pathway, and abnormal expression of ULK3 is associated with cancer [13, 14]. ULK3 is found to be an inducer of autophagy in human fibroblasts, which plays a key role in the activation of cancer associate fibroblasts [15, 16]. Researchers have found increased expression of the ULK3 kinase in cancer associate fibroblasts of various cancer types, while inhibition of its expression is associated with decreased tumor properties [17, 18]. Nevertheless, there is still a lack of systematic research on the role and molecular mechanism of ULK3-induced ER-phagy in prostate cancer.

This study tried to elucidate the mechanism that ULK3 promotes ER-phagy through the GLI1/CAMK2B pathway, which in turn leads to the malignant progression of prostate cancer, and provides a scientific basis for establishing ULK3 as a target for prostate cancer.

## Materials and methods

### *Ethics approval and patient sample collection*

Twelve pairs of tumor and adjacent normal tissue samples were obtained from prostate cancer patients in the First Affiliated Hospital of Wenzhou Medical University, and all patients signed the informed consent form. The information of clinical samples was provided in **Table 1**. Prostate cancer tissues and adjacent tissues were used for experimental studies. After cutting the collected samples, store them cryostead in liquid nitrogen at -80°C. All procedures involving human subjects were approved by the First Affiliated Hospital of Wenzhou Medical University Ethics Committee (YS2024-148), conducted in accordance with the ethics of the 1964 Declaration of Helsinki and its subsequent amendments and followed International Committee of Medical Journal Editors (ICMJE) recommendations.

### *Identification of key ER-phagy-related genes*

A set of 28 ER-phagy-related genes was collected from GeneCards by searching “Endoplasmic Reticulum Autophagy”, “Reticulophagy”, and “ER-phagy”. Their expression profiles in prostate cancer were examined using transcriptomic data from the TCGA-PRAD project. Differentially expressed genes (DEGs) between tumor and normal samples were called by limma ($|log2FC| > 1$, adjusted $P < 0.05$). Among the 28 candidates, four genes-SNX7, BCL2, CAMK2B, and ULK3-were identified as significantly upregulated. ULK3 displayed the greatest tumor-associated increase and the strongest clinical relevance. Importantly, a significant positive co-expression between ULK3 and CAMK2B was detected by Pearson correlation, pointing to a possible synergistic role in PCa progression. This led us to focus on the ULK3/CAMK2B axis.

### *Cell culture*

PC-3 and 22Rv-1 cells were obtained from the American Type Culture Collection (ATCC, Manassas, VA, USA). These cell lines were cultured according to our previous study [19].

### *Western blot*

Total proteins from cell and tissue samples were extracted using RIPA lysis buffer (Beyotime, China). For tissue samples, the specimens were initially snap-frozen in liquid nitrogen and pulverized into a fine powder using a mortar and pestle. Subsequently, the resulting cell or tissue lysates were incubated

on ice for 30 min, followed by centrifugation at 12,000 g for 15 min at 4°C to collect the supernatants. The supernatants were collected, and protein concentrations were quantified using a BCA protein assay kit (Beyotime, China). Protein samples were then mixed with 5× loading buffer at a 4:1 ratio and denatured at 95°C for 10 min. Equal amounts of protein from each group were separated via SDS-PAGE (Beyotime, China) and electrophoretically transferred onto PVDF membranes. The membranes were blocked with 5% non-fat milk for 1 h at room temperature and incubated overnight at 4°C with the corresponding primary antibodies. After incubation with horseradish peroxidase (HRP)-conjugated secondary antibodies (Abbkine, China), the protein bands were visualized using an enhanced chemiluminescence (ECL) kit (Thermo Fisher Scientific, USA). Primary antibody information was listed: ULK3 (1:2000, ab124947, Abcam, UK), CAMK2B (1:1000, 11533-1-AP, Proteintech, USA), Vimentin (1:1000, 60330-1-Ig, Proteintech, USA), E-cadherin (1:1000, 20874-1-AP, Proteintech, USA), p62 (1:1000, 18420-1-AP, Proteintech, USA), LC-3 (1:1000, NB100-2220, Novus Biologicals, USA), PRMT5 (1:1000, 18436-1-AP, Proteintech, USA), phospho-GLI1 (p-GLI1, 1:100, PA5105346, Fisher Scientific, USA), FAM134B (1:1000, 21537-1-AP, Proteintech, USA), SEC61B (1:1000, 1:1000, 60330-1-Ig, Proteintech, USA, Proteintech, USA), GLI1 (1:1000, NB600-600, Novus Biologicals, USA) and β-actin (1:20000, 66009-1-Ig, Proteintech, USA).

*Clone formation experiment*

Cells from each group were harvested and resuspended in complete medium containing 10% FBS (Gibco, USA). The cell suspension was serially diluted and seeded into 6-well plates at a density of 1,000 cells per well. The plates were then incubated at 37°C in a 5% $CO_2$ humidified atmosphere for 2 to 3 weeks until visible colonies were formed. Subsequently, the culture medium was discarded, and the adherent colonies were washed twice with PBS. The colonies were fixed with 4% paraformaldehyde (Beyotime, China) for 15 min at room temperature. After removal of the fixative, the cells were stained with 0.05% crystal violet (Beyotime, China) for 30 min. The excess dye was gently rinsed away with PBS, and the plates were allowed to air-dry. Finally, the colonies were photographed and the number of colonies was counted.

*Cell counting kit-8*

Cells in the logarithmic growth phase were harvested, counted, and seeded into 96-well plates at a density of $5*10^3$ cells/well. The plates were incubated at 37°C with 5% $CO_2$ for 24 h to allow for complete cell adherence. Following the designated treatments, 10 μL of CCK-8 reagent (Beyotime, China) was added to each well, and the plates were further incubated at 37°C for 2 h until a distinct orange-yellow color developed. Finally, the cell viability was evaluated by measuring the absorbance at 450 nm using a microplate reader.

*Transwell assay*

The cells were subjected to serum starvation for 24 h prior to the assay. The upper chambers of Transwell inserts (Corning, USA) were coated with Matrigel (Corning, USA) and incubated at 37°C for 2 h to allow polymerization. Subsequently, cells suspended in serum-free medium were seeded into the upper chambers, [while complete medium containing 10% FBS was added to the lower chambers as a chemoattractant]. After incubation for 24 h at 37°C, non-invading cells on the upper surface of the membrane were gently removed with a cotton swab. The invaded cells on the lower surface were then fixed with 4% paraformaldehyde (Beyotime, China) for 30 min, washed with PBS, and stained with crystal violet. Finally, the invaded cells were imaged and counted under a microscope.

*Wounding healing*

At 48 h post-transfection, cells reaching approximately 80% confluence were gently rinsed to remove residual serum and subjected to serum starvation for 12 h. Subsequently, the medium was discarded, and a sterile 200 μL pipette tip was held perpendicular to the plate to create a uniform scratch pattern across the center of each well [19]. The wells were then gently washed with PBS (Gibco, USA) to remove detached cells and cellular debris. The cells were further incubated in a medium supplemented with 1% FBS. Images of the scratch

intersections were captured at 0 and 24 h post-wounding.

*Immunofluorescence*

The LO2 cells were seeded in multi-well imaging plates and cultured to the desired confluence. After being washed twice with PBS, the cells were fixed with 4% paraformaldehyde for 15 min and permeabilized with 0.1% Triton X-100 (Beyotime, China) for 10 min. Following blocking with 5% BSA for 1 h, the cells were incubated overnight at 4°C with the following primary antibodies: anti-CAMK2B (1:100, 11533-1-AP, Proteintech), anti-PRMT5 (1:100, 18436-1-AP, Proteintech), and anti-GLI1 (1:100, N600-600, Novus Biologicals). Subsequently, the cells were incubated with fluorescently labeled secondary antibodies (Abbkine, China) in the dark. Nuclei were counterstained with DAPI for 5 min to indicate cell positioning. Fluorescence images were captured directly using a fluorescence microscope.

*Immunohistochemistry*

The paraffin-embedded sections were deparaffinized by baking at 60°C for 60 min, followed by rehydration through a graded series of ethanol. Endogenous peroxidase activity was quenched using a hydrogen peroxide block (Beyotime, China). For antigen retrieval, slides were immersed in sodium citrate buffer and heated in a microwave oven, then cooled to room temperature. After blocking with 5% BSA (Beyotime, China), the sections were incubated overnight at 4°C in a humidified chamber with the primary antibodies. Following three washes with PBS, the sections were incubated with secondary antibodies (Santa Cruz Biotechnology, USA). Signal detection was performed using a DAB substrate kit for 5 min, monitored under a microscope. Nuclei were counterstained with hematoxylin for 20 s. Finally, the slides were dehydrated, cleared, and mounted for observation under an optical microscope to evaluate protein distribution and expression. Primary antibody information was listed: ULK3 (1:200, ab124947, Abcam, UK), CAMK2B (1:100, 11533-1-AP, Proteintech, USA), GLI1 (1:200, NB600-600, Novus Biologicals, USA), Ki67 (1:4000, 27309-1-AP, Proteintech, USA), LC-3 (1:200, NB100-2220, Novus Biologicals, USA), Cleaved-Caspase3 (15 ug/mL, NBP3-48628, Novus Biologicals, USA), TUNEL (NBP2-31164, Novus Biologicals, USA) and FAM134B (1:1000, 21537-1-AP, Proteintech, USA).

*Cell transfection and lentiviral transduction*

Small interfering RNAs (siRNAs) targeting ULK3, CAMK2B, GLI1, and PRMT5, along with a negative control (si-NC), were synthesized by Genomeditech (Shanghai, China). Lentiviral vectors for target gene overexpression and knockdown were also constructed and packaged by Genomeditech. The specific target sequences are detailed in Table S1.

For transient gene knockdown, specific siRNAs were transfected into target cells (PC-3 and 22Rv-1) using the Lipofectamine 3000 reagent (Invitrogen, Waltham, MA, USA) according to the manufacturer's instructions.

To achieve stable gene expression or knockdown, target cells were transduced with lentiviral particles. To enhance transduction efficiency, 8 μg/mL polybrene (Sigma-Aldrich, USA) was added to the culture medium. After a 24-hour incubation, the medium was replaced with complete medium containing 2 μg/mL puromycin for resistance selection. The efficiency of overexpression or knockdown was subsequently validated by Western blot and qPCR.

*RT-PCR*

RT-PCR was performed according to previous study [20]. The sequences of primer were listed in Table S2.

*Chromatin Immunoprecipitation*

Chromatin Immunoprecipitation (CHIP) was carried out according to previous study [21].

*Co-Immunoprecipitation*

Co-Immunoprecipitation (COIP) was performed according to previous study [22]. Briefly, cell lysis buffer was prepared based on the protein source and interaction environment. The samples containing the target protein were mixed with the antibody-magnetic bead complex (Beyotime, China) to allow the target protein to bind to the antibody. Magnetic separation rack was used to separate unbound proteins from

the antibody-target protein complex, and impurities with wash buffer was removed. The Western blot was used to detect proteins that bind to the target protein.

*RNA sequencing and data analysis*

Total RNA was extracted from PC-3 cells transfected with si-NC or si-ULK3 (n = 3 per group) using Trizol reagent (Invitrogen, USA). Following RNA quality assessment (RIN ≥ 7.0), sequencing libraries were constructed using the TruSeq Stranded mRNA Kit (Illumina, USA) and sequenced on an Illumina NovaSeq 6000 platform to generate 150 bp paired-end reads. After removing adapters and low-quality reads, the clean reads were mapped to the human reference genome using HISAT2. Gene expression levels were quantified and normalized as transcripts per million (TPM). Differentially expressed genes (DEGs) between the two groups were identified using the limma R package. The thresholds for identifying significant DEGs were set as |log2(fold change)| > 1 and an adjusted *P*-value (FDR) < 0.05.

*In vivo models*

In Vivo Tumor Xenograft ModelMale BALB/c nude mice (4 weeks old) were purchased from the Laboratory Animal Center of the First Affiliated Hospital, Zhejiang University School of Medicine (Hangzhou, China). All animal experiments were performed in accordance with the International Guiding Principles for Biomedical Research Involving Animals and were approved by the Institutional Animal Care and Use Committee (IACUC) of Wenzhou Medical University (Approval No. wydw2024-0117). To establish the subcutaneous xenograft model, mice were randomly assigned into two groups (n = 5 per group). PC-3 cells (1*10^7) stably transfected with Lv-shNC or Lv-shULK3, suspended in 100 μL of PBS, were subcutaneously injected into the left axillary region of each mouse. Tumor dimensions were measured every 3 days using a digital vernier caliper. Tumor volume was calculated using the formula: V = (length*width^2)/2. At the end of the observation period, mice were euthanized via an isoflurane inhalation overdose. The xenograft tumors were then excised, photographed, weighed, and processed for subsequent analyses.

*Statistical analysis*

All statistical analyses were performed using GraphPad Prism 10 software (GraphPad Software, USA). Data are presented as the mean ± standard deviation (SD) from at least three independent experiments. For comparisons among multiple groups at a single time point, a one-way analysis of variance (ANOVA) followed by Tukey's multiple comparisons test was used. For experiments involving repeated measurements over time (e.g., CCK-8 assay, in vivo tumor volume measurement), a two-way repeated measures ANOVA (with time and group as factors) was applied, and Tukey's multiple comparisons test was used for post hoc analysis when appropriate. A paired Student's t-test was utilized for comparisons between paired tumor and adjacent normal tissues from the same patient. A *P*-value of < 0.05 was considered statistically significant.

## Results

*Four key genes of ER-phagy were identified*

Analysis of the TCGA database revealed that the expression levels of ER-phagy-related genes (*SNX7*, *BCL2*, *CAMK2B*, and *ULK3*) were significantly elevated in prostate cancer tissues. The distinct expression profiles of these four genes between normal and tumor tissues are illustrated in the heatmap (**Figure 1A**). Notably, ULK3 exhibited the most prominent upregulation. Further clinical correlation analysis demonstrated that ULK3 expression was consistently higher in tumor tissues across different age cohorts (41-60 and 61-80 years) compared to normal controls. When stratified by Gleason score, ULK3 expression was elevated across all tumor groups (scores 6-10) relative to normal tissues, peaking at a Gleason score of 8. Furthermore, based on the TCGA classification of prostate cancer into seven genetic subtypes (four driven by gene fusions and three characterized by *SPOP*, *FOXA1*, or *IDH1* mutations), ULK3 was significantly upregulated in fusion-driven subtypes compared to the normal group. Its expression was also uniformly elevated in both *TP53*-mutant and *TP53*-wildtype tumors. Additionally, ULK3 expression varied according to lymph node metastasis status, maintaining significantly

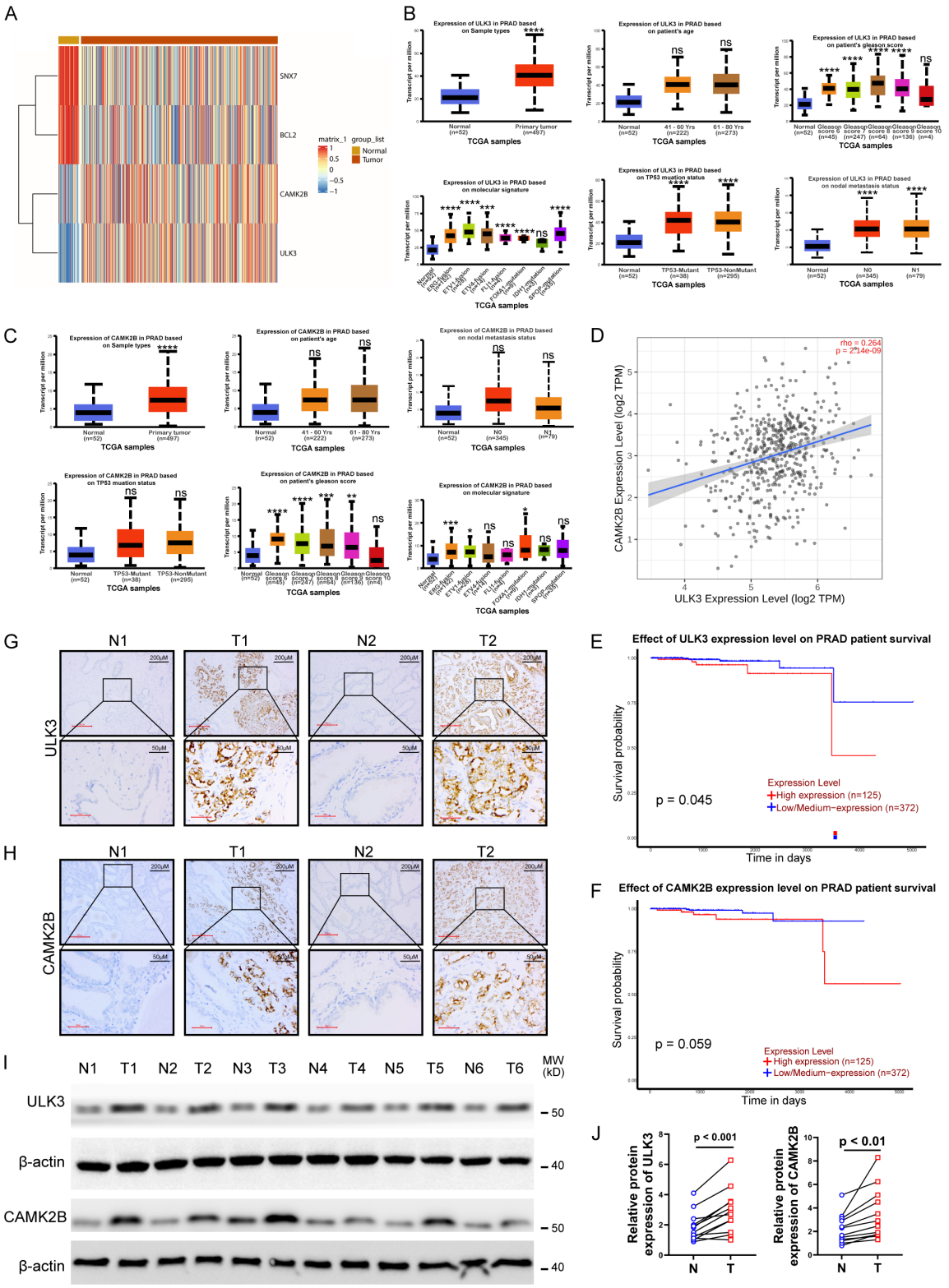


**Figure 1.** The key genes of prostate cancer related to ER-phagy were screened. A. The different expression of ER-phagy genes including SNX7, BCL2, CAMK2B and ULK3 in the TCGA prostate cancer database was demonstrated by heat map. B. Expression of ULK3 in PRAD was analyzed based on sample types, patient's age, patient's gleason score, molecular signature, TP53 mutation status, nodal metastasis status. C. Expression of CAMK2B in PRAD was analyzed according to sample types, patient's age, patient's gleason score, molecular signature, TP53 mutation

status, nodal metastasis status. D. Correlation analysis was performed for ULK3 and CAMK2B. E. Kaplan-Meier survival analysis result of ULK3 in PRAD. F. Kaplan-Meier survival analysis result of CAMK2B in PRAD. G. Immunohistochemistry was used to detect the protein content of ULK3 in normal and cancer tissues (n = 6). Scale bar = 200 (×5) or 50 (×20) μm. H. Immunohistochemistry was used to detect the protein content of CAMK2B and ULK3 in normal and cancer tissues. Scale bar = 200 (×5) or 50 (×20) μm. I. Western blot was used to detect the protein expression of ULK3 in twelve pairs of tumor and adjacent normal tissue samples (n = 12). J. Western blot was used to detect the protein expression of CAMK2B in twelve pairs of tumor and adjacent normal tissue samples (n = 12). Data were expressed as mean ± standard deviations. ***P < 0.001, **P < 0.01, *P < 0.05.

higher levels in both N0 and N1 stages compared to normal tissues (**Figure 1B**).

Subsequently, we analyzed the expression profiles of *CAMK2B* in PRAD based on sample type, *TP53* mutation status, patient age, molecular signatures, Gleason score, and lymph node metastasis status (**Figure 1C**). The expression pattern of *CAMK2B* across these clinical features closely mirrored that of *ULK3*. Indeed, Pearson correlation analysis revealed a significant positive correlation between *ULK3* and *CAMK2B* expression levels (**Figure 1D**). Furthermore, Kaplan-Meier survival analysis demonstrated that patients with high expression of either *ULK3* or *CAMK2B* exhibited a significantly poorer prognosis (**Figure 1E**, **1F**).

Building on these transcriptomic findings, we sought to validate them at the protein level. Accordingly, immunohistochemistry (IHC) revealed that ULK3 and CAMK2B were markedly elevated in tumor tissues (**Figure 1G**, **1H**). Consistent with these results, Western blot analysis confirmed the significant upregulation of ULK3 and CAMK2B proteins in prostate cancer tissues compared to adjacent normal tissues (**Figure 1I**, **1J**). Taken together, these findings strongly suggest a potential functional link between ER-phagy, ULK3, and CAMK2B in the progression of prostate cancer.

*Change of ULK3 expression effected the malignant progression of prostate cancer cells*

To elucidate the biological function of ULK3 in prostate cancer, we evaluated its effects on the malignant phenotypes of PC-3 and 22Rv-1 cells using loss- and gain-of-function approaches. First, the successful knockdown of ULK3 via small interfering RNA (siRNA) was confirmed by Western blot in both cell lines (**Figure 2A**). Functional assays revealed that ULK3 silencing significantly impaired cell viability (**Figure 2B**) and suppressed clonogenic capacity (**Figure 2C**). Furthermore, Transwell and wound healing assays demonstrated a marked reduction in the invasive (**Figure 2D**) and migratory (**Figure 2E**) abilities of ULK3-depleted cells, respectively. Conversely, to assess the impact of ULK3 upregulation, we established stable ULK3-overexpressing cells via lentiviral transduction (Lv-ULK3), which was verified at the protein level (**Figure 2F**). ULK3 overexpression robustly promoted cell proliferation (**Figure 2G**) and dramatically enhanced cell invasion (**Figure 2H**). Moreover, overexpression of ULK3 significantly accelerated cell migration, as evidenced by increased wound closure rates (**Figures 2I** and S2B).

Taken together, these data indicate that ULK3 acts as a crucial driver, promoting the growth, proliferation, and mobility of prostate cancer cells.

*Inhibition of ULK3 suppressed CAMK2B mRNA expression*

To further elucidate the regulatory mechanisms linking ULK3 and CAMK2B, transcriptome sequencing (RNA-seq) was conducted on PC-3 cells following ULK3 knockdown. Transcriptomic profiling demonstrated that ULK3 depletion significantly downregulated CAMK2B mRNA expression (**Figure 3A** and **3B**). Additionally, KEGG and GSEA enrichment analyses revealed that the AMPK and cAMP signaling pathways were highly enriched upon ULK3 inhibition, suggesting that phosphorylation events may contribute to ULK3-mediated regulation in prostate cancer (**Figure 3C** and **3D**). Consistent with the RNA-seq findings, quantitative real-time PCR (qRT-PCR) confirmed a marked reduction in CAMK2B mRNA levels in si-ULK3-transfected cells (**Figure 3E**). To assess whether ULK3 transcriptionally regulates CAMK2B, chromatin immunoprecipitation (ChIP) assays were performed. The results indicated that ULK3 does not physically bind to

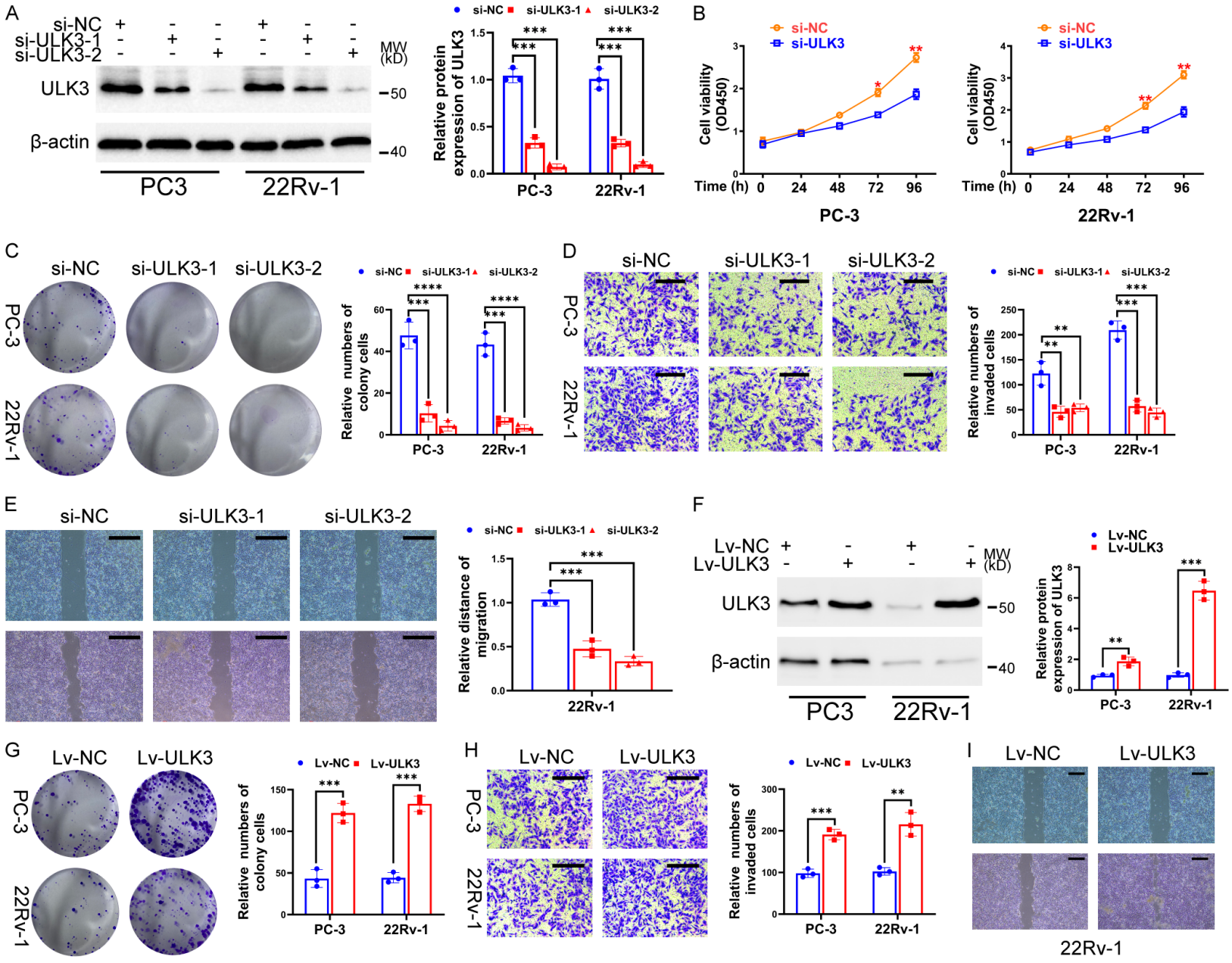
A
si-NC
si-ULK3-1
si-ULK3-2
MW (kD)
ULK3
β-actin
50
40
PC3
22Rv-1
Relative protein expression of ULK3
PC-3
22Rv-1
B
si-NC
si-ULK3
Cell viability (OD450)
Time (h)
PC-3
22Rv-1
C
si-NC
si-ULK3-1
si-ULK3-2
PC-3
22Rv-1
Relative numbers of colony cells
D
Relative numbers of invaded cells
E
Relative distance of migration
F
Lv-NC
Lv-ULK3
G
H
I

**Figure 2.** After inhibition of ULK3, the malignant characteristics of PC-3 and 22Rv-1 cells was suppressed. A. Western blot was used to detect ULK3 protein expression levels of PC-3 and 22Rv-1 in prostate cancer cells. B. CCK-8 assay was used to detect cell viability. C. Colony formation experiment was used to detect the proliferation ability of cells. D. Transwell assay was employed to examine the invasive capacity of PC-3 and 22Rv-1 cells. Scale bar = 100 (×10) μm. E. Wounding healing assay was utilized to detect the migration ability of 22Rv-1 cells. Scale bar = 200 (×5) μm. F. Western blot was utilised to detect ULK3 protein expression levels in prostate cancer cells. G. Clone formation assay was employed to detect the proliferation ability of PC-3 and 22Rv-1 in prostate cancer cells. H. Transwell assay was utilized to detect the invasive capacity of cancer cells. Scale bar = 100 (×10) μm. I. Wounding healing assay was employed to detect the migration ability of cancer cells. Scale bar = 200 (×5) μm. Data were expressed as mean ± standard deviations. ****P < 0.0001, ***P < 0.001, **P < 0.01, *P < 0.05.

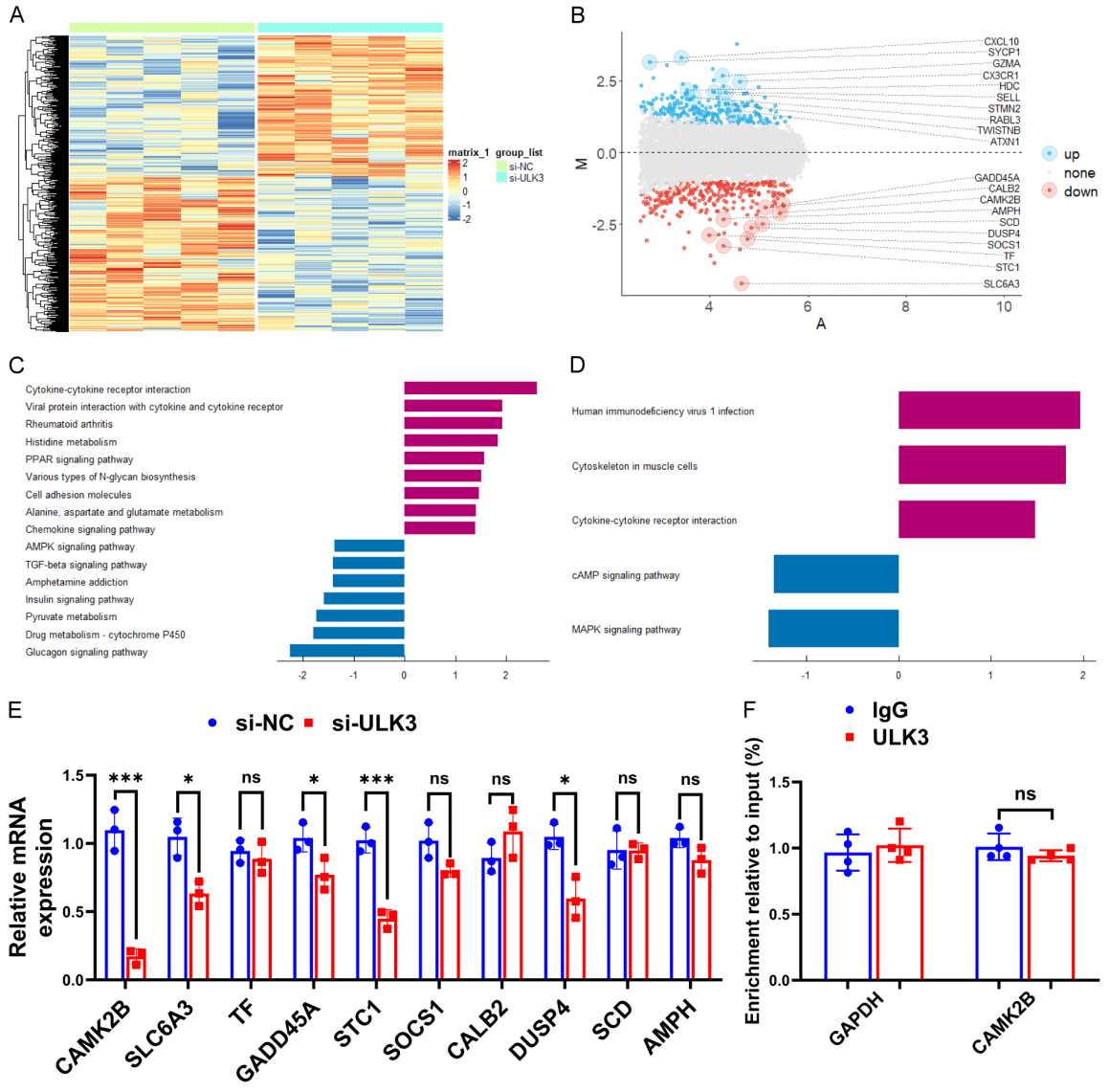


**Figure 3.** Transcriptome sequencing was performed. A. Differential genes were displayed in the heatmap. B. Top 10 down-regulated genes and up-regulated genes were displayed in the volcano plot. C. KEGG analysis were performed. D. GSEA analysis were performed. E. RT-PCR results were showed in Histogram. F. CHIP results were showed in Histogram. Data were expressed as mean ± standard deviations. ***P < 0.001, **P < 0.01, *P < 0.05.

the CAMK2B promoter, suggesting that ULK3 regulates CAMK2B indirectly rather than through direct transcriptional activation (**Figure 3F**).

*Change of CAMK2B expression effected the function of ULK3*

Afterwards, we tried to understand the relationship between ULK3 and CAMK2B in prostate cancer cells through western blot and immunofluorescence assay. After down-regulation of ULK3, the expression of CAMK2B in PC-3 was significantly reduced (**Figure 4A**). Up-regulation of ULK3 increased the expression of CAMK2B (Figure S2A). Immunofluorescence assay was used to detect the expression and localization of CAMK2B. CAMK2B protein expression exhibited a notable decline because of the decrease in ULK3 expression (**Figure 4B**).

Western blot, clone formation experiment, transwell assay and Wound healing assay were carried out after overexpression of CAMK2B. Western blot indicated that CAMK2B protein levels was remarkably reduced after knockdown of CAMK2B by si-CAMK2B (**Figure 4C**). After transfection of Lv-CAMK2B, CAMK2B protein was abundantly overexpressed (**Figure 4D**). Transwell, clone formation and Wound healing assay were performed to detect the malignant function of prostate cancer cells after inhibition and overexpression of CAMK-2B. After inhibition of CAMK2B, the number of clones of prostate cancer cells was significantly reduced, and the cell invasive ability and proliferation ability were also weakened (**Figure 4E-G**). After overexpression of CAMK2B, we obtained the opposite experimental results, with a significant increase in the number of prostate cancer cell clones, and an increase in cell invasion and proliferation (**Figure 4H-J**). The above experimental results indicated that CAMK2B significantly accelerated the proliferation of cancer cells and had a promoting effect on prostate cancer cells.

*ULK3 affected positively prostate cancer cell vitabity by regulating CAMK2B*

After confirming that both ULK3 and CAMK2B are involved in prostate cancer progression, we performed a series of multi-group controlled experiments to dissect the functional relationship between ULK3 and CAMK2B in PC-3 cells. Knockdown of ULK3 markedly reduced the proliferative, invasive, and migratory capacities of PC3 cells, and these impairments were effectively reversed by CAMK2B overexpression (**Figure 5A**, **5C**, **5E**, **5G**, **5I**, **5K**). Conversely, ULK3 overexpression significantly enhanced proliferation, invasion, and migration, whereas these pro-tumorigenic effects were attenuated in the si-CAMK2B group (**Figure 5B**, **5D**, **5F**, **5H**, **5J**, **5L**). Elevated Vimentin expression has been documented in various malignancies, including prostate and breast cancers [25], and functional studies have corroborated its tumor-promoting role [18]. Following ULK3 overexpression, Vimentin protein levels increased in the NC control group but were notably diminished in the si-CAMK2B group. In parallel, E-cadherin protein expression was significantly decreased upon ULK3 overexpression in NC cells, whereas it was restored in the si-CAMK2B group (**Figure 5M**, **5N**). Collectively, these findings indicate that ULK3 promotes prostate cancer cell aggressiveness in a CAMK2B-dependent manner.

*ULK3 promotes the phosphorylation of GLI1 to facilitate its entry into the nucleus, inducing the transcription of CAMK2B*

To determine whether ULK3 physically interacts with GLI1 or PRMT5 in prostate cancer cells, we performed co-immunoprecipitation (Co-IP) assays. The results demonstrated that ULK3 binds specifically to GLI1. No detectable interaction with PRMT5 was observed (**Figure 6A**, **6B**). Knockdown of ULK3 did not alter the total expression level of PRMT5. However, inhibition of p-GLI1 markedly attenuated the ULK3-induced upregulation of CAMK2B. Notably, inhibition of PRMT5 failed to produce a similar effect (**Figure 6C-F**). Immunofluorescence analysis further revealed that ULK3 overexpression promoted the nuclear accumulation of GLI1, whereas it had no discernible effect on the subcellular localization of PRMT5 (**Figure 6E-I**). Chromatin immunoprecipitation (ChIP) assays indicated that GLI1 directly binds to the promoter region of CAMK2B (**Figure 6J**). Moreover, inhibition of GLI1 abolished the proliferative and migratory capacities driven by ULK3 overexpression (**Figure 6K**, **6L**). Taken together, these findings indicate that ULK3 enhances CAMK2B transcription by phosphorylating GLI1, thereby facilitating its nuclear entry and subsequent binding to the CAMK2B promoter.

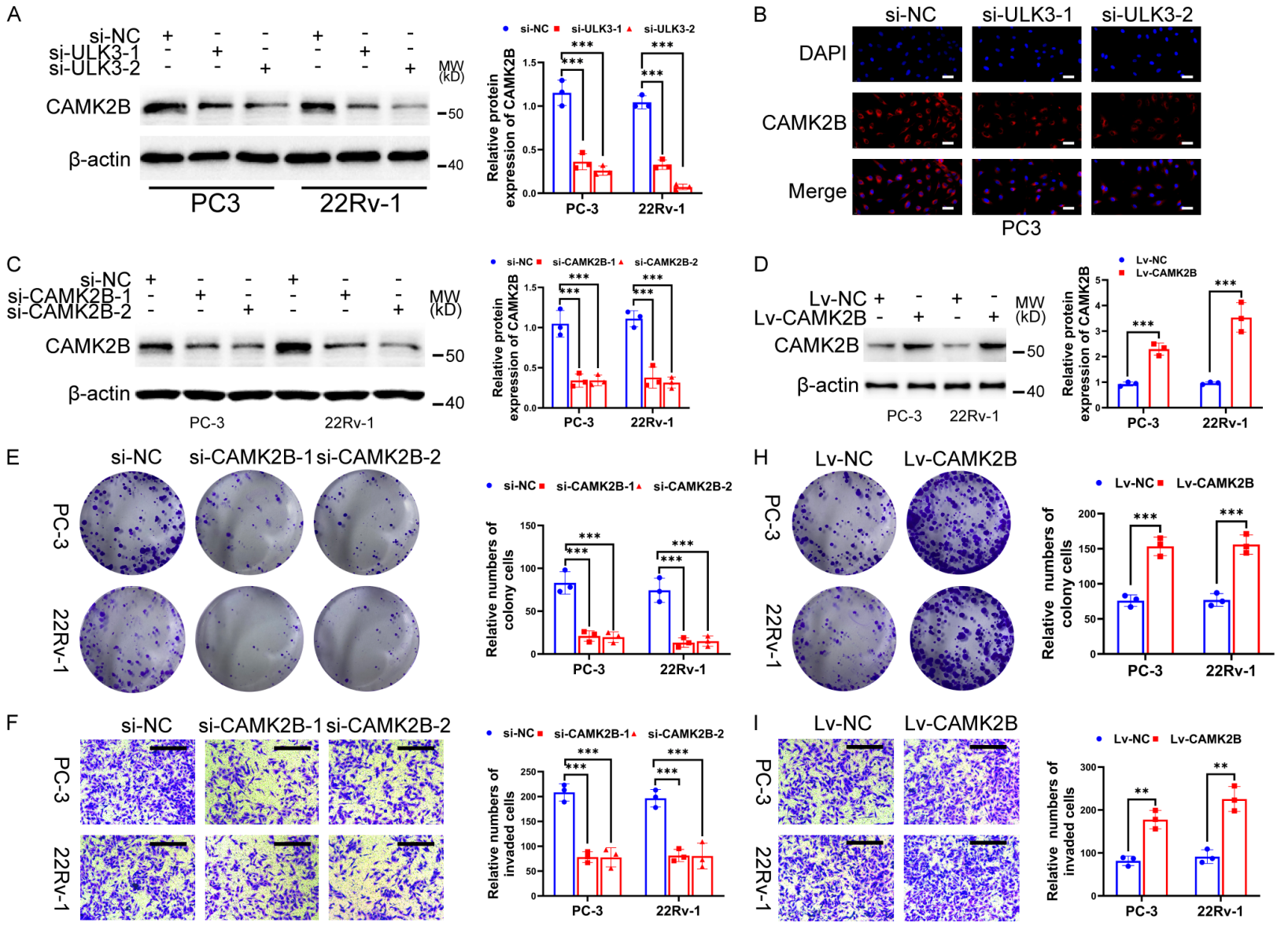
A
si-NC
si-ULK3-1
si-ULK3-2
MW (kD)
CAMK2B
β-actin
50
40
PC3
22Rv-1
Relative protein expression of CAMK2B
PC-3
22Rv-1
B
si-NC
si-ULK3-1
si-ULK3-2
DAPI
CAMK2B
Merge
PC3
C
si-CAMK2B-1
si-CAMK2B-2
D
Lv-NC
Lv-CAMK2B
E
F
H
I
Relative numbers of colony cells
Relative numbers of invaded cells

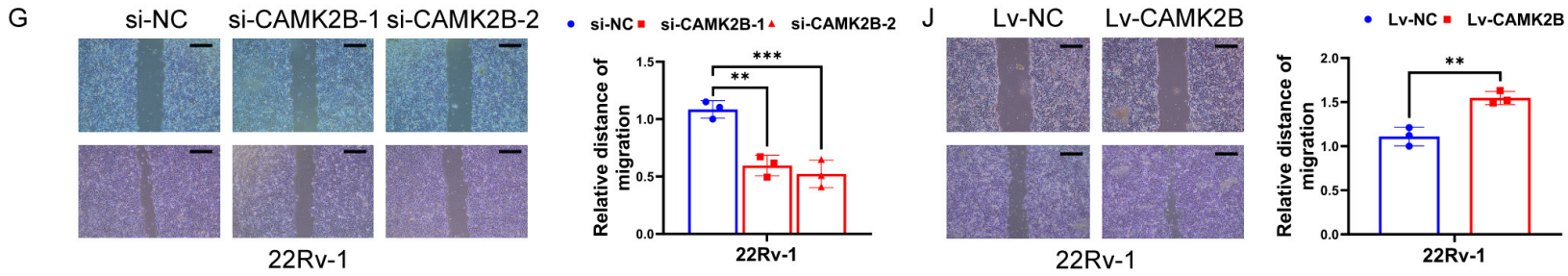


**Figure 4.** CAMK2B promoted the proliferation, invasion and migration of prostate cancer cells. A. Western blot was used to detect the protein expression level of CAMK2B in prostate cancer cells. B. Detection of CAMK2B expression and localization was performed by Immunofluorescence assay. scale bar = 20 (×40) μm. C. The CAMK2B protein expression level of PC-3 and 22Rv-1 cells was measured by Western blot. D. After overexpression of CAMK2B, the CAMK2B protein expression level of PC-3 and 22Rv-1 cells was detected by Western blot. E. The number of clones in PC-3 and 22Rv-1 cells after inhibition of CAMK2B was detected by clone formation experiment. F. After inhibition of CAMK2B, invasion of 22Rv1 cells was measured by Transwell assay. Scale bar = 100 (×10) μm. G. After inhibition of CAMK2B, migration of 22Rv1 cells was measured by wounding healing assay. Scale bar = 100 (×10) μm. H. Clone formation experiment was used to detect the number of clones of PC-3 and 22Rv-1 in prostate cancer cells after overexpressing CAMK2B. I. Transwell assay was used to detect the invasion of prostate cancer cells after overexpression of CAMK2B. Scale bar = 100 (×10) μm. J. After overexpression of CAMK2B, migration of 22Rv1 cells was detected by Wounding healing. Scale bar = 200 (×5) μm. Data were expressed as mean ± standard deviations. ***P < 0.001, **P < 0.01, *P < 0.05.

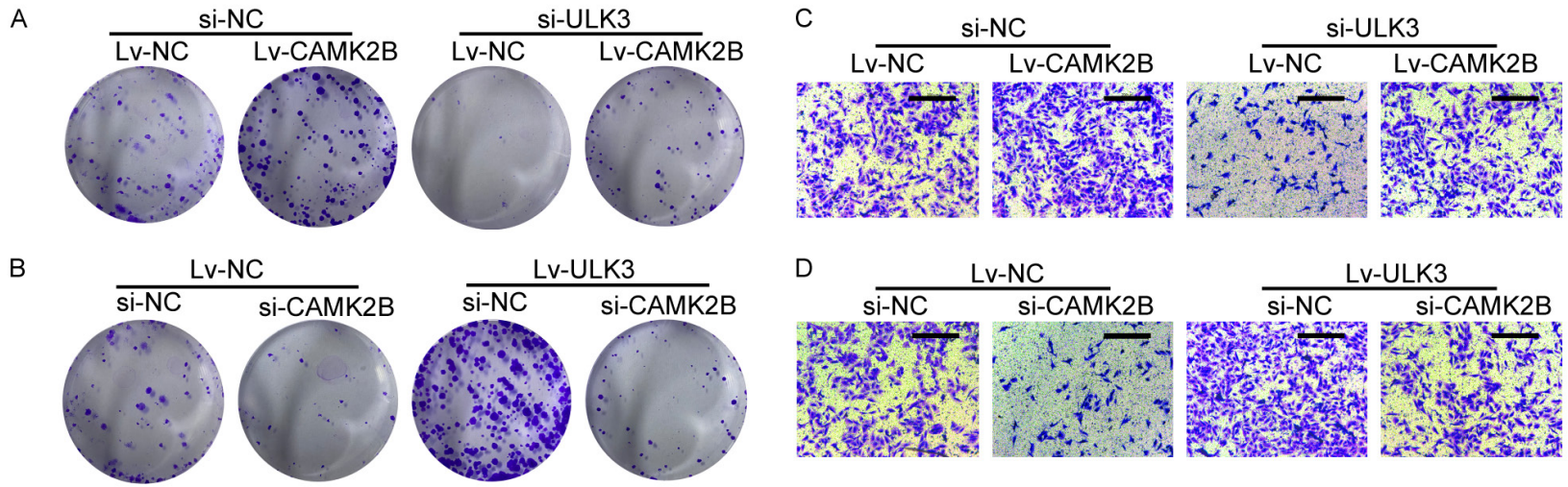

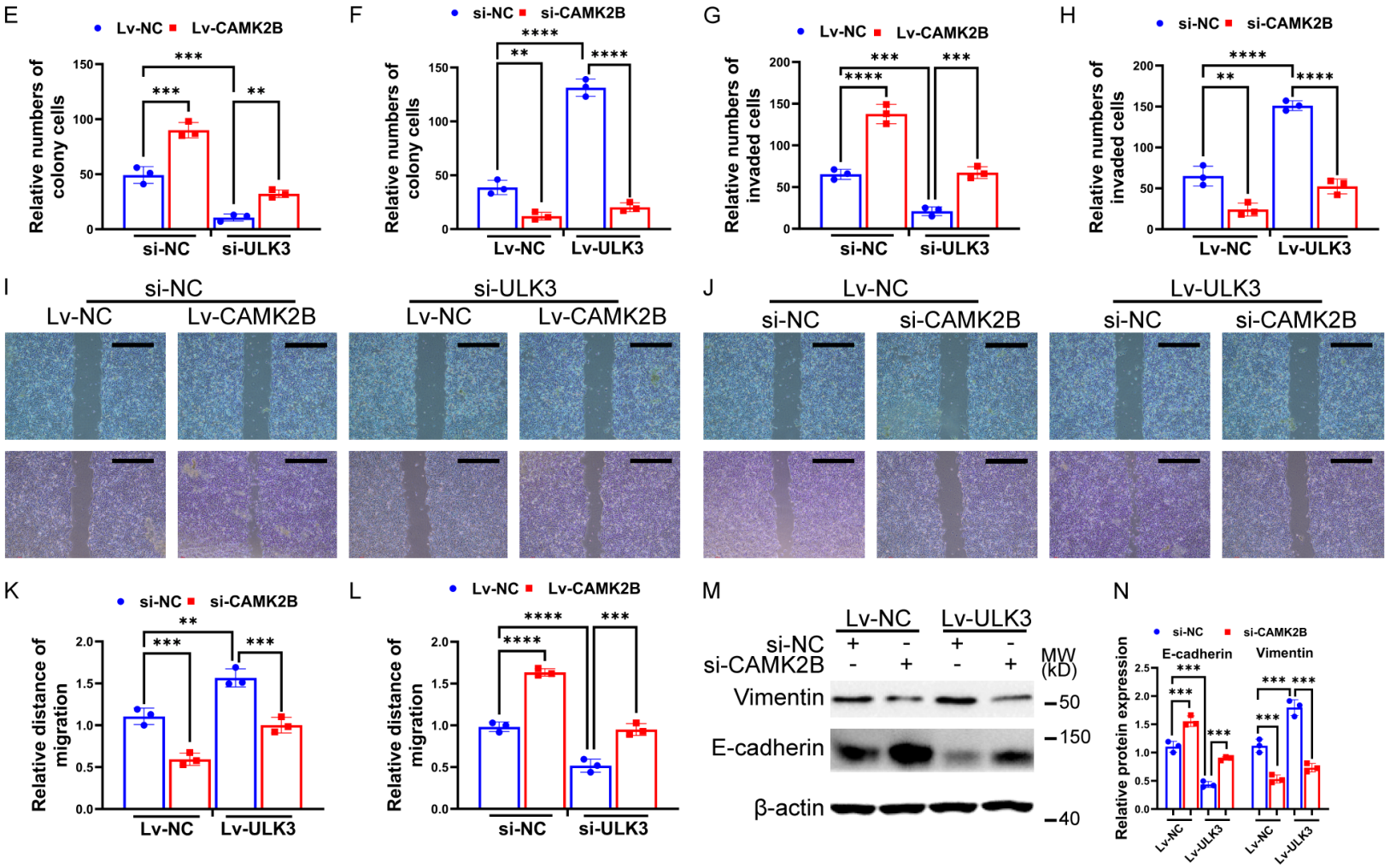


**Figure 5.** CAMK2B could reversed the effect of ULK2 in PC-3 cells. A. After knockdown of ULK3, the difference in the number of cancer cell clones between the NC control group and the Lv-CAMK2B group was compared. B. After overexpression of ULK3, the difference in the number of cancer cell clones between NC control group and si-CAMK2B group was compared. C. After inhibition of ULK3, the cancer cell invasion of the NC control group and the lv-CAMK2B group were compared. Scale bar = 100 (×10) μm. D. After ULK3 overexpression, the cancer cell invasion was compared between the NC control group and the si-CAMK2B group. Scale bar = 100 (×10) μm. E. The histogram was used to show the clone formation results. F. The histogram was employed to show the clone formation results. G, H. The histogram was utilized to show the Transwell assay results. I. Cancer cell migration after ULK3 overexpression was compared between the NC control group and the si-CAMK2B group. Scale bar = 200 (×5) μm. J. After knockdown of ULK3, the migration of cancer cells in the NC control group and the Lv-CAMK2B group was compared. Scale bar = 200 (×5) μm. K, L. The histogram was used to show the results of the clone formation experiment. M. ULK3 was overexpressed, and the protein expression of E-cadherin and Vimentin in NC control group and si-CAMK2B group was compared. N. The histogram was applied to showed the Western blot results. Data were expressed as mean ± standard deviations. ****P < 0.0001, ***P < 0.001, **P < 0.01, *P < 0.05.

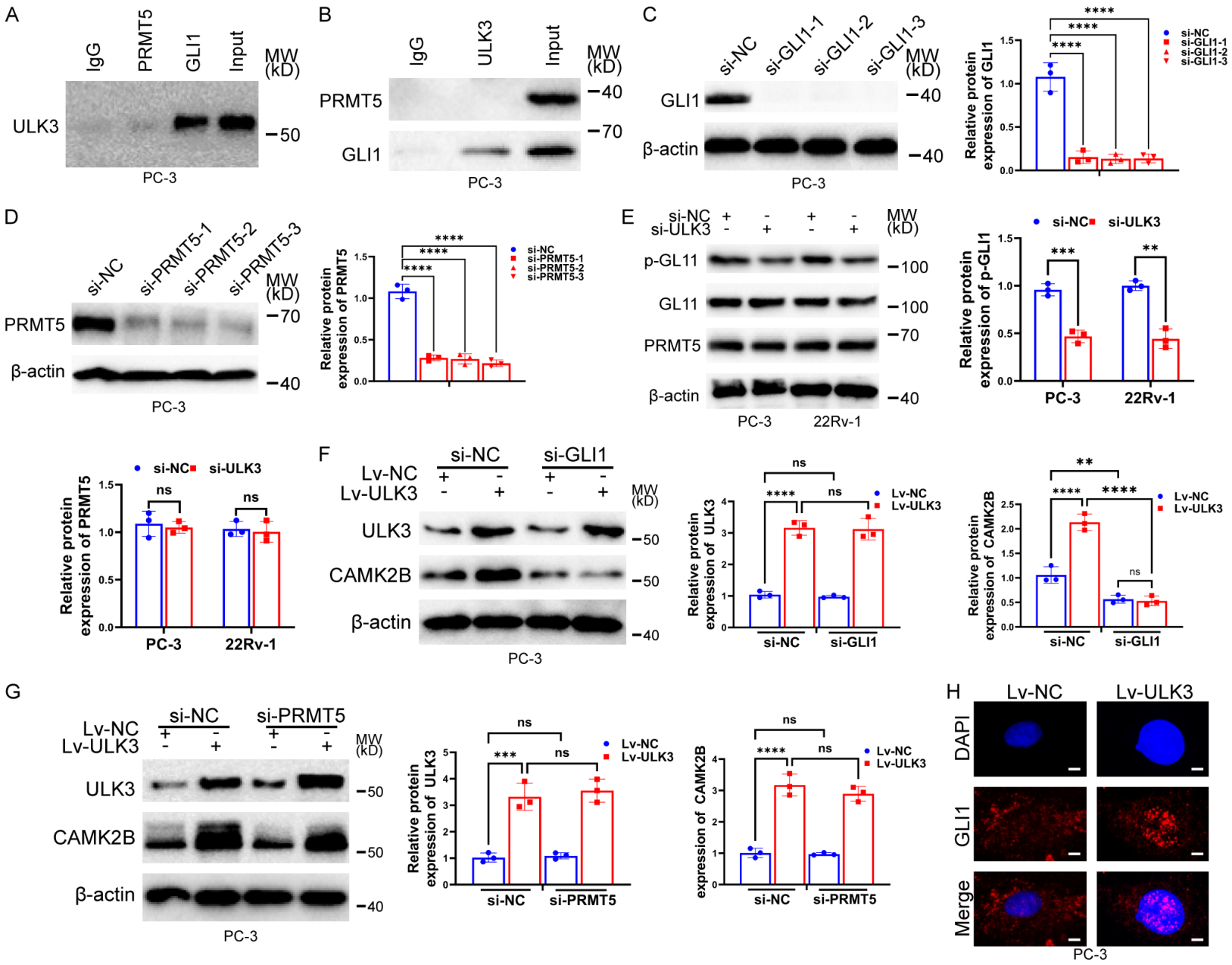
A
IgG
PRMT5
GLI1
Input
MW (kD)
ULK3
50
PC-3
B
IgG
ULK3
Input
MW (kD)
PRMT5
40
70
GLI1
PC-3
C
si-NC
si-GLI1-1
si-GLI1-2
si-GLI1-3
MW (kD)
GLI1
40
β-actin
40
PC-3
Relative protein expression of GLI1
si-NC
si-GLI1-1
si-GLI1-2
si-GLI1-3
D
si-NC
si-PRMT5-1
si-PRMT5-2
si-PRMT5-3
MW (kD)
PRMT5
70
β-actin
40
PC-3
Relative protein expression of PRMT5
si-NC
si-PRMT5-1
si-PRMT5-2
si-PRMT5-3
E
si-NC
si-ULK3
MW (kD)
p-GL11
100
GL11
100
PRMT5
70
β-actin
40
PC-3
22Rv-1
Relative protein expression of p-GLI1
si-NC
si-ULK3
PC-3
22Rv-1
Relative protein expression of PRMT5
si-NC
si-ULK3
ns
PC-3
22Rv-1
F
Lv-NC
Lv-ULK3
si-NC
si-GLI1
MW (kD)
ULK3
50
CAMK2B
50
β-actin
40
PC-3
Relative protein expression of ULK3
Lv-NC
Lv-ULK3
si-NC
si-GLI1
Relative protein expression of CAMK2B
Lv-NC
Lv-ULK3
si-NC
si-GLI1
G
Lv-NC
Lv-ULK3
si-NC
si-PRMT5
MW (kD)
ULK3
50
CAMK2B
50
β-actin
40
PC-3
Relative protein expression of ULK3
Lv-NC
Lv-ULK3
si-NC
si-PRMT5
expression of CAMK2B
Lv-NC
Lv-ULK3
si-NC
si-PRMT5
H
Lv-NC
Lv-ULK3
DAPI
GLI1
Merge
PC-3

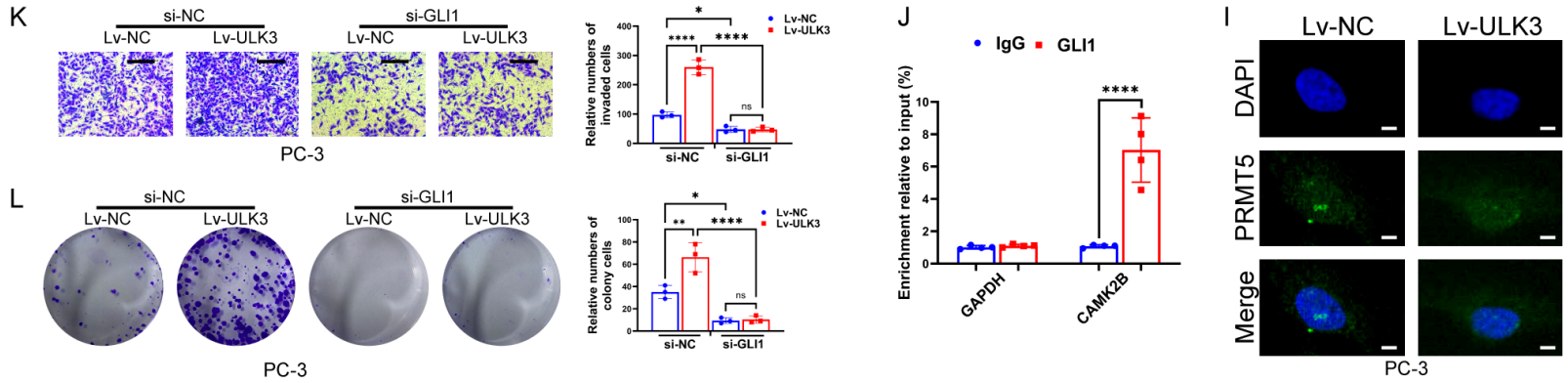


**Figure 6.** ULK3 promotes the nuclear entry of GLI1 and increases the transcription of CAMK2B. A, B. COIP was used to detect the binding between ULK3, GLI1 and PRMT5 in PC-3 cells. C. The knockdown of GLI1 was confirmed by Western blot in PC-3 cells. D. The knockdown of PRMT5 was confirmed by Western blot in PC-3 cells. E. The p-GLI1, GLI1 and PRMT5 protein expression was determined by Western blot after ULK3 knockdown in PC-3 and 22Rv-1 cells. F. ULK3 and CAMK2B protein expression were detected by Western blot in PC-3 cells. Cells were transfected Lv-ULK3 and then si-GLI1. G. ULK3 and CAMK2B protein expression were detected by Western blot in PC-3 cells. Cells were transfected Lv-ULK3 and then si-PRMT5. H. Detection of GLI1 expression and localization was performed by Immunofluorescence assay after transfection of Lv-ULK3, Scale bar = 5 (×200) μm. I. Detection of GLI1 expression and localization was performed by Immunofluorescence assay after transfection of Lv-ULK3. Scale bar = 5 (×200) μm. J. CHIP results were showed in Histogram. K. Invasion of PC-3 cells were detected by Transwell assays. Cells were transfected Lv-ULK3 and then si-GLI1. Scale bar = 100 (×10) μm. L. Proliferation of PC-3 cells were detected by colony formation assays. Cells were transfected Lv-ULK3 and then si-GLI1. ****P < 0.0001, ***P < 0.001, **P < 0.01, *P < 0.05.

*ULK3 mediated CAMK2B-induced ER-phagy to promote the malignant progression of prostate cancer*

To further delineate the regulatory roles of ULK3 and CAMK2B in ER-phagy within prostate cancer cells, we performed a series of functional assays. The proteins p62 and LC3-II are well-established markers of autophagic activity. Following ULK3 knockdown, the protein levels of both p62 and LC3-II were markedly reduced. This result indicates an impairment in basal autophagic activation (**Figure 7A**).

We next examined the impact of ULK3 on ER-phagy-specific receptors. Overexpression of ULK3 resulted in a marked accumulation of LC3-II. FAM134B mRNA expression in PRAD differed from ULK3 and CAMK2B in that it was not significantly difference in adjacent tissues and in prostate cancer tissues (Figure S1A). Interestingly, SEC61B mRNA expression in PRAD was upregulated (Figure S1B). At the same time, the protein levels of p62, FAM134B, and SEC61B decreased. These changes indicate enhanced ER-phagy. Importantly, these dynamic changes were robustly abrogated by CAMK2B knockdown (**Figure 7B**, **7D**).

We next sought to confirm that the reduction in ER components was due to active autophagic flux rather than transcriptional downregulation. To this end, we used bafilomycin A1 (Baf), a late-stage inhibitor of autophagosome-lysosome fusion (**Figure 7C**, **7E**). Baf treatment elicited a marked accumulation of LC3-II, p62, FAM134B, and SEC61B. This accumulation effectively prevented the degradation promoted by ULK3 overexpression. These findings strongly support the notion that ULK3 facilitates active ER turnover. This turnover occurs through lysosome-dependent ER-phagy.

Finally, we asked whether this process is functionally linked to tumor progression. We used rapamycin, a classical autophagy inducer, to address this question. CAMK2B knockdown severely suppressed the clonogenic survival of prostate cancer cells. It also reduced their invasive capacity. However, pharmacological induction of autophagy with rapamycin significantly rescued these malignant phenotypes (**Figure 7F-I**). Collectively, our results demonstrate that the ULK3/CAMK2B signaling axis promotes prostate cancer progression. It does so by driving ER-phagy.

*The results of ULK3 inhibited the vitality of prostate cancer tumors in vivo*

To validate the in vitro findings, we established a subcutaneous xenograft mouse model. Two groups of PC-3 cells were prepared. One group carried stable ULK3 knockdown (Lv-shULK3). The other group served as the control (Lv-shNC). Cells were injected subcutaneously into the flanks of mice. Tumors were allowed to grow for 35 days.

The results showed that tumors in the Lv-shULK3 group were significantly smaller than those in the control group. Specifically, the average tumor weight in the control group was about three times that of the knockdown group. Tumor volume in the control group was roughly twice as large (**Figure 8A-C**). Western blot analysis confirmed that ULK3 and CAMK2B protein levels were markedly reduced in tumor tissues from the Lv-shULK3 group (**Figure 8D**, **8E**).

Immunohistochemistry (IHC) analysis provided further evidence. ULK3 depletion significantly lowered the protein levels of ULK3, CAMK2B, and LC3 in tumor tissues. In contrast, the level of FAM134B, an ER-phagy receptor, increased significantly (**Figure 8F**). Nuclear GLI1 expression was also visibly decreased (**Figure 8G**). Notably, Ki67 expression declined in the Lv-shULK3 group. This finding indicates suppressed cell proliferation. However, no significant differences were observed in Cleaved-caspase3 or TUNEL staining between the two groups (**Figure 8G**).

These results demonstrate that ULK3 downregulation curbs tumor growth mainly by inhibiting cell proliferation. It does not appear to induce apoptosis. In summary, ULK3 promotes the malignant progression of prostate cancer. It does so by driving ER-phagy through the GLI1/CAMK2B signaling axis.

## Discussion

Prostate cancer (PCa) ranks among the most common and deadly cancers in men. Endocrine therapy and radical surgery work well at first. Yet most patients later develop castration-

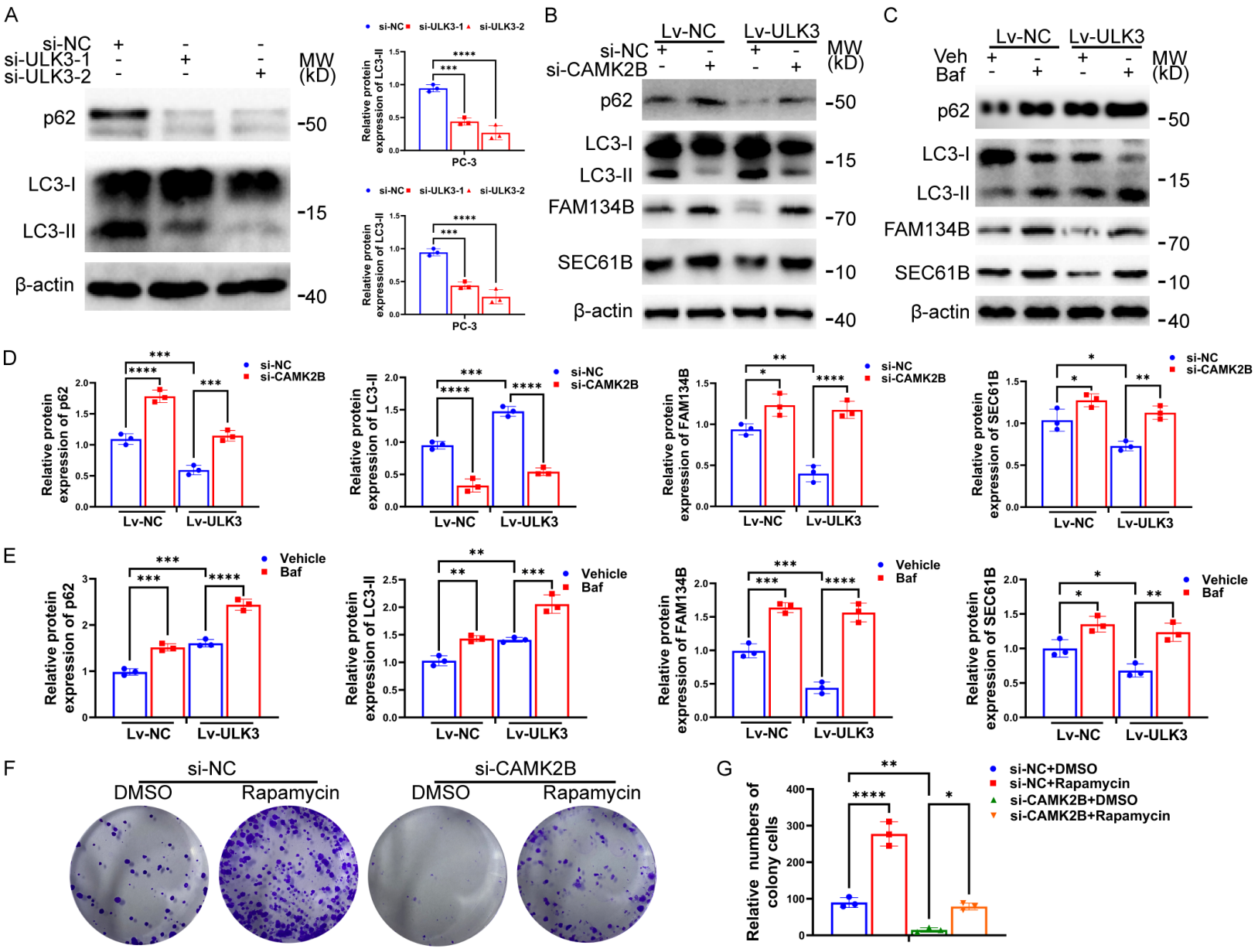
A
si-NC
si-ULK3-1
si-ULK3-2
MW (kD)
p62
LC3-I
LC3-II
β-actin
-50
-15
-40
si-NC si-ULK3-1 si-ULK3-2
Relative protein expression of LC3-II
PC-3
B
Lv-NC
Lv-ULK3
si-CAMK2B
FAM134B
SEC61B
-70
-10
C
Veh
Baf
D
Relative protein expression of p62
Relative protein expression of LC3-II
Relative protein expression of FAM134B
Relative protein expression of SEC61B
si-NC
si-CAMK2B
E
Vehicle
Baf
F
si-NC
si-CAMK2B
DMSO
Rapamycin
G
Relative numbers of colony cells
si-NC+DMSO
si-NC+Rapamycin
si-CAMK2B+DMSO
si-CAMK2B+Rapamycin

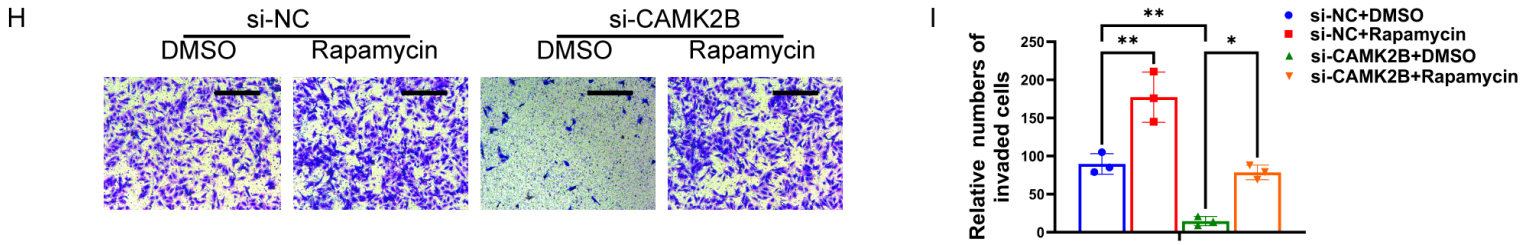


**Figure 7.** The relationship between ULK3, CAMK2B and ER-phagy in prostate cancer was analyzed. A. After inhibition of ULK3, Western blot was performed to detect the protein expression of p62, LC3-I and LC3-II, which were key molecules of autophagy. B. The protein expressions of p62, LC3-I, LC3-II, FAM134B and SEC61B, which were key molecules of ER-phagy in the si-NC and the si-CAMK2B group were detected after ULK3 overexpression. C. The protein expressions of p62, LC3-I, LC3-II, FAM134B and SEC61B, which were key molecules of ER-phagy in the vehicle and bafilomycin A1 (Baf, 3 nM) group were detected after ULK3 overexpression. D, E. The histogram was used to show the protein expressions of p62, LC3-I, LC3-II, FAM134B and SEC61B. F. After inhibiting CAMK2B, the number of cell clones in DMSO group and Rapamycin group was compared. G. The clone formation experiment results were shown in the histogram. H. After knockdown of CAMK2B, the cell invasion of DMSO group and Rapamycin group were compared. Scale bar = 100 (×10) μm. I. The histogram showed the Transwell assays results. Data were expressed as mean ± standard deviations. ****P < 0.0001, ***P < 0.001, **P < 0.01, *P < 0.05.

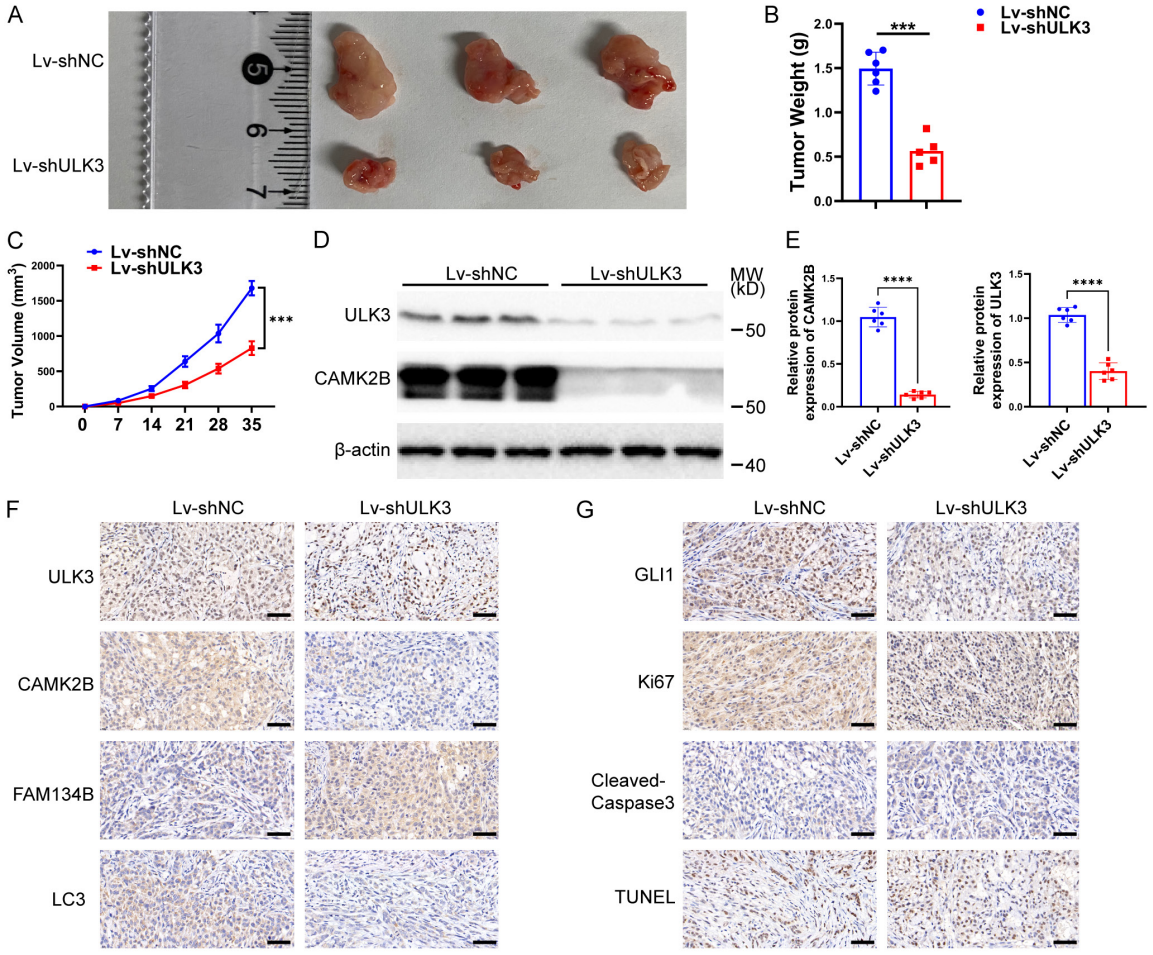


**Figure 8.** The changes in tumors and corresponding genes were compared after subcutaneous injection of lv-shULK3 into prostate cancer cells *in vivo*. A. Tumor sizes *in vivo* were analyzed. B. Histogram was utilized to displayed the changes in tumor weight in figure. C. Histogram was employed to show the change in tumor volume. D. The protein changes of ULK3 and CAMK2B were analyzed by Western blot. E. Histogram was used to show the protein changes of ULK3 and CAMK2B. F. The protein changes of ULK3, CAMK2B, FAM134B and LC3 were detected by Immunohistochemistry. Scale bar = 20 (×40) μm. G. The protein changes of GLI1, Ki67, Cleaved-caspase3 and TUNEL were detected by Immunohistochemistry. Sscale bar = 20 (×40) μm. Data were expressed as mean ± standard deviations. ****P < 0.0001, ***P < 0.001, **P < 0.01, *P < 0.05.

resistant prostate cancer (CRPC) and metastasis [23, 24]. New molecular drivers of PCa malignancy are urgently needed. Endoplasmic reticulum (ER)-phagy is a selective form of autophagy. It acts as a double-edged sword in cancer. Cancer cells often use ER-phagy to clear damaged ER. This reduces cellular stress and gives them a survival edge in harsh conditions [25]. In this study, we identified a new regulatory axis. This axis-ULK3/GLI1/CAMK2B-strongly drives PCa progression. It does so by boosting ER-phagy.

We analyzed transcriptomic data from the TCGA database. Four ER-phagy-related genes stood out. These were SNX7, BCL2, CAMK2B, and ULK3. All four were significantly upregulated in PCa tissues. Clinical correlation showed that higher ULK3 expression is tied to worse outcomes. It links to advanced Gleason scores, lymph node spread, and poor prognosis. ULK1 is well studied [7]. The role of ULK3 in cancer was less clear. Our functional assays, both in vitro and in vivo, gave clear answers. ULK3 depletion cut down PCa cell proliferation and invasion. It also slowed xenograft tumor growth. ULK3 overexpression had the opposite effect. It boosted all these oncogenic traits. These data establish ULK3 as a key oncogenic driver in prostate cancer. They also back up

earlier reports. Those reports linked ULK3 to cancer-associated fibroblast activation and tumor growth [18].

Next, we asked how ULK3 drives this malignant phenotype. We saw a strong positive link between ULK3 and CAMK2B expression. However, ChIP assays ruled out one idea. ULK3 does not act as a direct transcription factor on the CAMK2B promoter. ULK3 is a serine/threonine kinase. So we looked at its downstream phosphorylation targets. Co-IP and immunofluorescence data gave us a clue. ULK3 physically binds to GLI1. It also helps GLI1 move into the nucleus. Once inside the nucleus, GLI1 binds the CAMK2B promoter. This turns on CAMK2B transcription. This is a key finding. It elegantly ties the Hedgehog/GLI1 pathway to ULK3 kinase activity. This creates an indirect but powerful network that drives CAMK2B overexpression.

We found that ER-phagy is the final step of this pathway. Earlier work shows CAMK2B triggers ER-phagy [26]. It does so by phosphorylating FAM134B, an ER receptor. This phosphorylation cuts the ER into pieces. Our transcriptomic data showed FAM134B mRNA levels stay flat between normal and tumor tissues. In contrast, SEC61B mRNA is clearly upregulated. At the protein level, ULK3 overexpression sped things up. It caused faster breakdown of FAM134B, SEC61B, and p62. LC3-II piled up at the same time. This degradation was blocked by bafilomycin A1, a lysosome inhibitor. This proves the drop in ER proteins comes from active autophagy [27]. It is not due to less transcription. The gap between mRNA and protein levels points to one thing. Post-translational changes, like phosphorylation by CAMK2B, matter most here. We used rapamycin to turn on autophagy. This treatment restored the growth and invasion lost after CAMK2B knockdown. This confirms that ER-phagy is the main event. It links ULK3/CAMK2B signals to cancer cell behavior.

Our study has some limits. We could not find good commercial antibodies for phosphorylated PRMT5. So we could not measure its levels. PRMT5 is another possible target of ULK3. Because of this, we cannot fully rule out PRMT5 effects. It might work together with GLI1 or act as a backup route. Also, FAM134B and SEC61B both get eaten up during ER-phagy. Yet they may have different jobs. For example, SEC61B might act as a calcium channel [28]. It could let calcium leak out of the ER. How these two receptors work together in ULK3-driven ER-phagy is still unclear. Future studies will need to sort out their exact roles. Furthermore, although our findings indicate that CAMK2B mediates ER-phagy and involves the degradation of FAM134B, another limitation of this study is the lack of direct experimental evidence confirming the physical interaction between CAMK2B and FAM134B. Additionally, we did not utilize kinase-dead mutants of ULK3 or CAMK2B in our current experiments. Therefore, the exact post-translational modification mechanisms, particularly whether CAMK2B directly phosphorylates FAM134B to trigger ER-phagy, remain to be definitively verified. Future investigations employing kinase-inactive mutants and direct binding assays, such as Co-Immunoprecipitation (Co-IP) or pull-down assays, are required to fully elucidate these specific phosphorylation cascades.

In conclusion, our work maps out a new oncogenic axis. This axis runs from ULK3 to GLI1 to CAMK2B and ends in ER-phagy. Blocking this pathway could disrupt the stress-handling tricks of cancer cells. This makes it a very promising target for treating advanced prostate cancer.

## Conclusion

This article showed that ULK3 induced ER-phagy by mediating the GLI1/CAMK2B signaling pathway to promote the malignant progression of prostate cancer and provided new insights for the study of prostate cancer, which could be combined with existing treatment methods to better treat prostate cancer patients.

## Disclosure of conflict of interest

None.

**Address correspondence to:** Hui-Liang Zhou and Qin-Quan Wang, Department of Andrology and Sexual Medicine, The First Affiliated Hospital of Fujian Medical University, 20 Chazhong Road, Fuzhou 350005, Fujian, China. E-mail: zhlpaper@fjmu.edu.cn (HLZ); wangqinquan@wzhospital.cn (QQW)

## References


[1] Virtanen V, Paunu K, Ahlskog JK, Varnai R, Sipeky C and Sundvall M. PARP inhibitors in prostate cancer-the preclinical rationale and current clinical development. Genes (Basel) 2019; 10: 565.

[2] Scher HI and Heller G. Clinical states in prostate cancer: toward a dynamic model of disease progression. Urology 2000; 55: 323-327.

[3] Rosellini M, Santoni M, Mollica V, Rizzo A, Cimadamore A, Scarpelli M, Storti N, Battelli N, Montironi R and Massari F. Treating prostate cancer by antibody-drug conjugates. Int J Mol Sci 2021; 22: 1551.

[4] Torre LA, Bray F, Siegel RL, Ferlay J, Lortet-Tieulent J and Jemal A. Global cancer statistics, 2012. CA Cancer J Clin 2015; 65: 87-108.

[5] Fararjeh AS and Liu YN. ZBTB46, SPDEF, and ETV6: novel potential biomarkers and therapeutic targets in castration-resistant prostate cancer. Int J Mol Sci 2019; 20: 2802.

[6] Sekhoacha M, Riet K, Motloung P, Gumenku L, Adegoke A and Mashele S. Prostate cancer review: genetics, diagnosis, treatment options, and alternative approaches. Molecules 2022; 27: 5730.

[7] Zhou H, Wang K, Wang M, Zhao W, Zhang C, Cai M, Qiu Y, Zhang T, Shao R and Zhao W. ER-phagy in the occurrence and development of cancer. Biomedicines 2022; 10: 707.

[8] Mowers EE, Sharifi MN and Macleod KF. Functions of autophagy in the tumor microenvironment and cancer metastasis. FEBS J 2018; 285: 1751-1766.

[9] Li YJ, Lei YH, Yao N, Wang CR, Hu N, Ye WC, Zhang DM and Chen ZS. Autophagy and multidrug resistance in cancer. Chin J Cancer 2017; 36: 52.

[10] Levine B and Kroemer G. Biological functions of autophagy genes: a disease perspective. Cell 2019; 176: 11-42.

[11] Antunes F, Erustes AG, Costa AJ, Nascimento AC, Bincoletto C, Ureshino RP, Pereira GJS and Smaili SS. Autophagy and intermittent fasting: the connection for cancer therapy? Clinics (Sao Paulo) 2018; 73: e814s.

[12] Goruppi S, Clocchiatti A, Bottoni G, Di Cicco E, Ma M, Tassone B, Neel V, Demehri S, Simon C and Paolo Dotto G. The ULK3 kinase is a determinant of keratinocyte self-renewal and tumorigenesis targeting the arginine methylome. Nat Commun 2023; 14: 887.

[13] Liu B, Gao W, Sun W, Li L, Wang C, Yang X, Liu J and Guo Y. Promoting roles of long non-coding RNA FAM83H-AS1 in bladder cancer growth, metastasis, and angiogenesis through the c-Myc-mediated ULK3 upregulation. Cell Cycle 2020; 19: 3546-3562.

[14] Maloverjan A, Piirsoo M, Michelson P, Kogerman P and Osterlund T. Identification of a novel serine/threonine kinase ULK3 as a positive regulator of Hedgehog pathway. Exp Cell Res 2010; 316: 627-637.

[15] Guttieri L, Raffa S, Salerno G, Bigi R, Persechino F, Visco V, Torrisi MR, Ranieri D and Belleudi F. FGFR2c upregulation contributes to cancer-associated fibroblast program activation and to enhanced autophagy in actinic keratosis-derived dermal fibroblasts: a possible role in precancerous cell/stromal cell crosstalk. Biology (Basel) 2023; 12: 463.

[16] Cui K, He J, Zhao N, Ma R and Wang Y. Bioinformatics analysis identifies ULK3 as a novel prognostic and immune-related biomarker in esophageal cancer. Transl Cancer Res 2025; 14: 6588-6604.

[17] Young AR, Narita M, Ferreira M, Kirschner K, Sadaie M, Darot JF, Tavaré S, Arakawa S, Shimizu S, Watt FM and Narita M. Autophagy mediates the mitotic senescence transition. Genes Dev 2009; 23: 798-803.

[18] Goruppi S, Procopio MG, Jo S, Clocchiatti A, Neel V and Dotto GP. The ULK3 kinase is critical for convergent control of cancer-associated fibroblast activation by CSL and GLI. Cell Rep 2017; 20: 2468-2479.

[19] Lin Q, Cai J and Wang QQ. The significance of circular RNA DDX17 in prostate cancer. Biomed Res Int 2020; 2020: 1878431.

[20] Xu WN, Zheng HL, Yang RZ, Sun YF, Peng BR, Liu C, Song J, Jiang SD and Zhu LX. The mitochondrial UPR induced by ATF5 attenuates intervertebral disc degeneration via cooperating with mitophagy. Cell Biol Toxicol 2024; 40: 16.

[21] Xu WN, Zheng HL, Yang RZ, Liu T, Yu W, Zheng XF, Li B, Jiang SD and Jiang LS. Mitochondrial NDUFA4L2 attenuates the apoptosis of nucleus pulposus cells induced by oxidative stress via the inhibition of mitophagy. Exp Mol Med 2019; 51: 1-16.

[22] Xu WN, Liu C, Zheng HL, Xu HX, Yang RZ, Jiang SD and Zhu LX. Sesn2 serves as a regulator between mitochondrial unfolded protein response and mitophagy in intervertebral disc degeneration. Int J Biol Sci 2023; 19: 571-592.

[23] Siegel R, Ma J, Zou Z and Jemal A. Cancer statistics, 2014. CA Cancer J Clin 2014; 64: 9-29.

[24] Ferlay J, Steliarova-Foucher E, Lortet-Tieulent J, Rosso S, Coebergh JW, Comber H, Forman D and Bray F. Cancer incidence and mortality patterns in Europe: estimates for 40 countries in 2012. Eur J Cancer 2013; 49: 1374-1403.

[25] Studer UE, Hauri D, Hanselmann S, Chollet D, Leisinger HJ, Gasser T, Senn E, Trinkler FB, Tscholl RM, Thalmann GN and Dietrich D. Immediate versus deferred hormonal treatment

for patients with prostate cancer who are not suitable for curative local treatment: results of the randomized trial SAKK 08/88. J Clin Oncol 2004; 22: 4109-4118.

[26] Jiang X, Wang X, Ding X, Du M, Li B, Weng X, Zhang J, Li L, Tian R, Zhu Q, Chen S, Wang L, Liu W, Fang L, Neculai D and Sun Q. FAM134B oligomerization drives endoplasmic reticulum membrane scission for ER-phagy. EMBO J 2020; 39: e102608.

[27] Cui J, Liu J, Fan L, Zhu Y, Zhou B, Wang Y, Hua W, Wei W and Sun G. A zinc finger family protein, ZNF263, promotes hepatocellular carcinoma resistance to apoptosis via activation of ER stress-dependent autophagy. Transl Oncol 2020; 13: 100851.

[28] Parys JB and Van Coppenolle F. Sec61 complex/translocon: the role of an atypical ER Ca2+-leak channel in health and disease. Front Physiol 2022; 13: 991149.

**Table S1.** The sequence of Si-RNA

| Si-RNA | Sequence (5'-3') |
|---|---|
| si-NC | 5'-UUCUCCGAACGUGUCACGU-3' |
| si-ULK3-1 | 5'-GCAGACUUUGGUUUCGCAC-3' |
| si-ULK3-2 | 5'-GCAAGGCUCUGGACUUCUU-3' |
| si-CAMK2B-1 | 5'-GACCAGATGTGATTTGTTAAA-3' |
| si-CAMK2B-2 | 5'-GATCATTAAGACCACGGAGCA-3' |
| si-GLI1-1 | 5'-GCAAAUAGGGCUUCACAUA-3' |
| si-GLI1-2 | 5'-AGGCUCAGCUUGUGUGUAA-3' |
| si-GLI1-3 | 5'-GGACGAGGGACCUUGCAUU-3' |
| si-PRMT5-1 | 5'-GCCCAGUUUGAGAUGCCUU-3' |
| si-PRMT5-2 | 5'-CCGCUAUUGCACCUUGGAA-3' |
| si-PRMT5-3 | 5'-GGGACUGGAAUACGCUAAUTT-3' |

**Table S2.** The list of primer sequences for qRT-PCR

| GENE | Sequence (5'-3') |
|---|---|
| CAMK2B-F | 5'-TACTTCGAGAACCTGCTGGC-3' |
| CAMK2B-R | 5'-TGAGCCGGATGTAAGCGATG-3' |
| TF-F | 5'-CCGTCCTGGGGCTGTG-3' |
| TF-R | 5'-ACAAGCAACACTGGGACCAT-3' |
| SLC6A3-F | 5'-GCCTACATCTTCCCCGACTG-3' |
| SLC6A3-R | 5'-GCGTAGGCCAGTTTCTCTCG-3' |
| GADD45A-F | 5'-CAGAAGACCGAAAGCGACCC-3' |
| GADD45A -R | 5'-CAGAAGACCGAAAGCGACCC-3' |
| STC1-F | 5'-TGAAGTGGTTCGTTGCCTCA-3' |
| STC1-R | 5'-GACGAATGCTTTTCCCTGAGT-3' |
| SOCS1-F | 5'-TTTTCGCCCTTAGCGTGAAGA-3' |
| SOCS1-R | 5'-GAGGCAGTCGAAGCTCTCG-3' |
| CALB2-F | 5'-AGAGATGTCCCGACTCCTGC-3' |
| CALB2-R | 5'-TCGTAAAATGTGAAGATCGCGT-3' |
| DUSP4-F | 5'-TGCCTGCTCAAAGGCGG-3' |
| DUSP4-R | 5'-AAGGATCTCCACAGGACCCC-3' |
| SCD-F | 5'-GTGATGTTCCAGAGGAGGTACT-3' |
| SCD-R | 5'-CGCAAGAAAGTGGCAACGAA-3' |

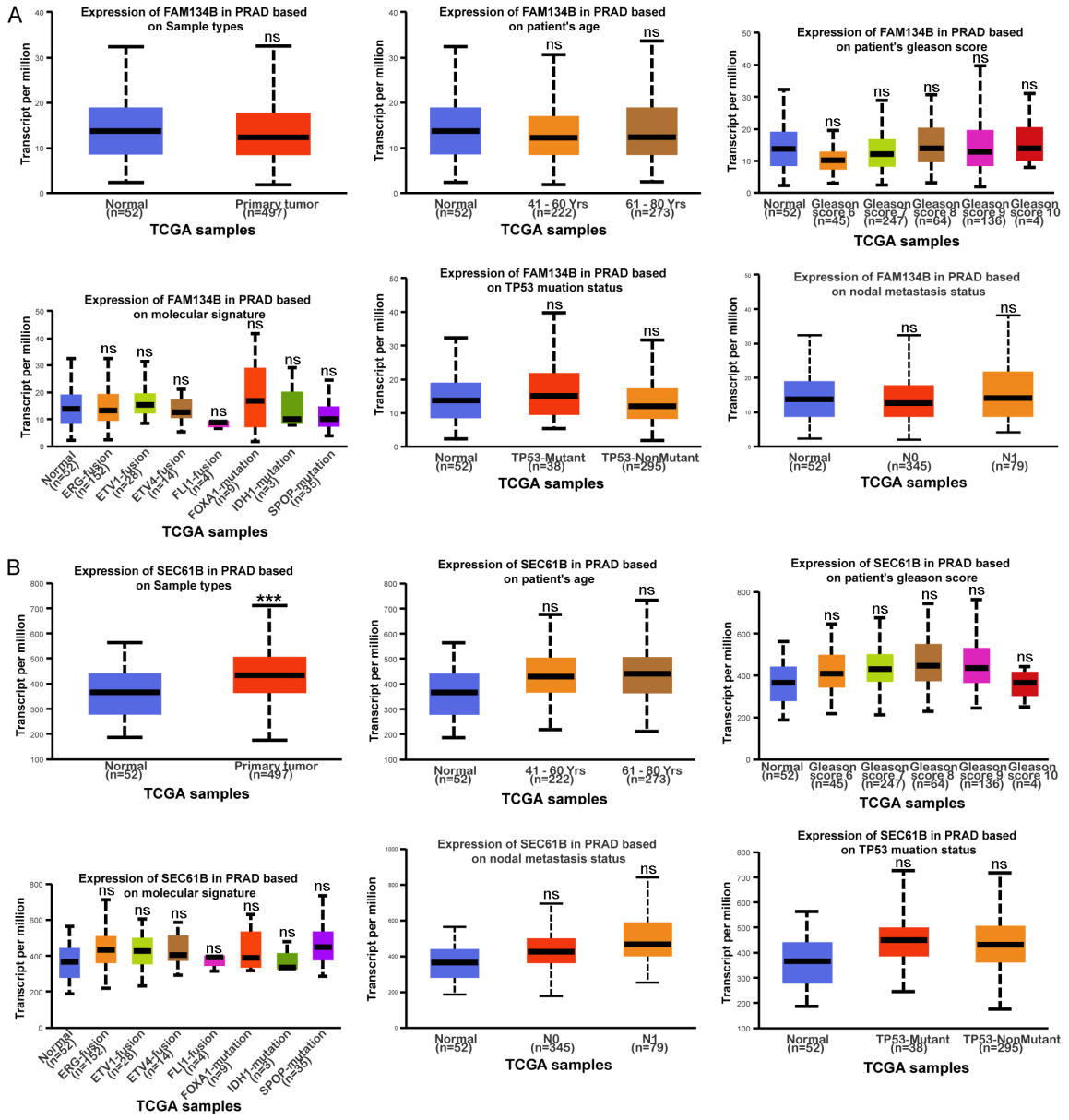


**Figure S1.** A. Expression of FAM134B in PRAD was analyzed based on sample types, patient's age, patient's gleason score, molecular signature, TP53 mutation status, nodal metastasis status. B. Expression of SEC61B in PRAD was analyzed according to sample types, patient's age, patient's gleason score, molecular signature, TP53 mutation status, nodal metastasis status.

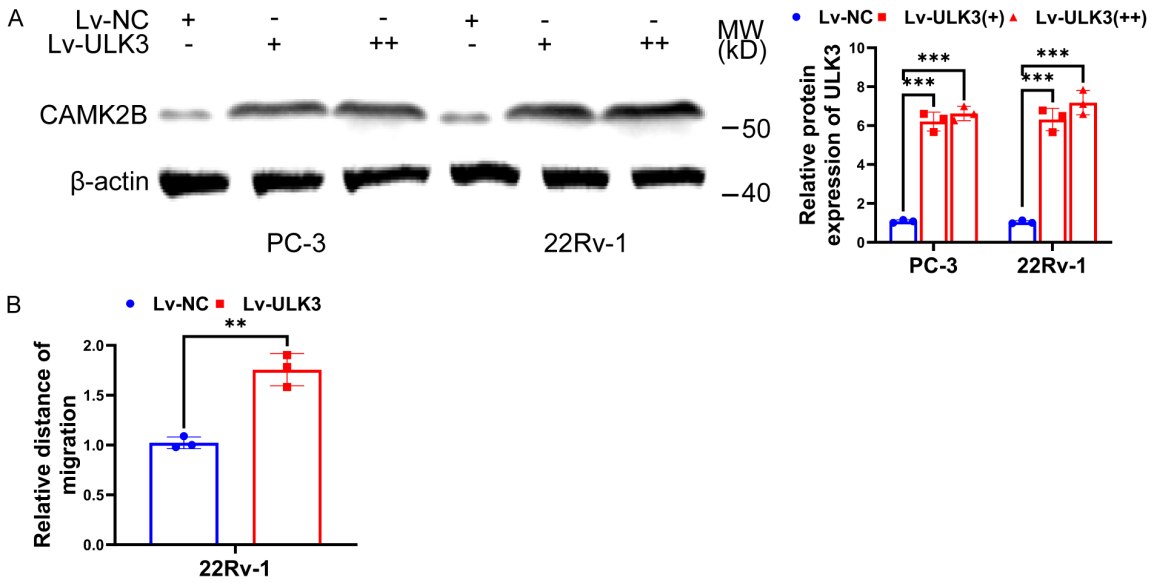


**Figure S2.** A. Western blot was used to detect the protein expression level of CAMK2B in prostate cancer cells. B. Histogram was used to show the results of the wounding healing assay.